Bottom-up and top-down control in a multitrophic system: the role of nutrient limitation and infochemical-mediated predation in a plankton food-web model

Nicola D. Walker[1*], Hadi Susanto[2], Michael Steinke[3], Edward A. Codling[2]**
[1]Centre for Environment, Fisheries and Aquaculture Science (Cefas)
Pakefield Road, NR33 0HT, United Kingdom
[2]Department of Mathematical Sciences, University of Essex,
Wivenhoe Park, Colchester, CO4 3SQ, United Kingdom
[3]School of Biological Sciences, University of Essex,
Wivenhoe Park, Colchester, CO4 3SQ, United Kingdom
Email: **ecodling@essex.ac.uk

Abstract

Chemicals released following herbivore grazing on primary producers can promote multitrophic interactions by influencing the foraging behaviour of higher order predators. In particular, chemicals released during microzooplankton grazing on phytoplankton can act as infochemical cues that elicit foraging responses and improve search efficiency in carnivorous copepods. Models investigating such infochemical-mediated multitrophic interactions in the plankton are typically based on top-down control, where phytoplankton concentrations are controlled through predation and grazing from higher trophic levels. However, in marine environments nutrient limitation is an important factor that influences a food-web from below, and earlier models of this system only indirectly account for this by assuming predator-free growth is logistic with a fixed carrying capacity. Here we consider the dynamics of infochemical-mediated interactions in a marine system where nutrient limitation is modelled directly through an extended NPZ-style model. We show the one-parameter bifurcation behavior of the top-down model to change when the total nutrient availability is changed, and hence demonstrate phytoplankton bloom formation to be a function of both top-down and bottom-up processes.

Keywords: Plankton dynamics, Infochemicals, NPZ-model, Population dynamics, Food-webs, Multitrophic interactions
2010 MSC: 34K18, 34K20, 34K60, 92D40

1. INTRODUCTION

Primary producers employ numerous, sophisticated defense systems in response to grazers. In particular, marine phytoplankton have been shown to employ morphological defenses, e.g. [15], and can respond to the threat of predation by changing their behavior, e.g. [17] or life history [e.g. by adjusting recruitment; 16]. Phytoplankton also employ chemical defenses against grazers, such as deterrents, e.g. [42] and toxins, e.g. [38] which, in addition to these bitrophic interactions, may span multiple trophic levels by indirectly influencing the foraging behavior of higher order predators [35].

Here we consider interactions where microzooplankton grazing on phytoplankton causes the release of infochemical cues that attract predatory copepods to prey on microzooplankton, subsequentlyy reducing grazing on phytoplankton and promoting multitrophic interactions. Phytoplankton produce a wide range of chemical products that could potentially mediate such multitrophic interactions, an example of which is dimethylsulphide (DMS). DMS is well known for its potential impact in climate regulation [4] and is also now known to be an important marine infochemical, with many recent studies reporting attraction by numerous taxa, e.g. [31, 21, 11]. The release of DMS is known to increase rapidly when microzooplankton graze on phytoplankton [1, 43] and can elicit a behavioral foraging response in the copepod *Temora longicornis* [36], making it a relevant example for this study.

---

*née Lewis
**Corresponding author
Received April 23^{th}, 2019, Revised July 23^{th}, 2019, Accepted for publication July 25^{th}, 2019. e-ISSN: 2549-2896, DOI:10.5614/cbms.2019.2.2.1

Lewis et al. [24] considered a model of the interactions between phytoplankton, microzooplankton and copepods where interactions were mediated by infochemicals produced when microzooplankton graze on phytoplankton. The inclusion of an infochemical term in their model had a stabilizing effect on the resultant population dynamics and acted to promote phytoplankton bloom formation [24]. Extensions of this work have considered phytoplankton competition [25] and vertical heterogeneity [26]. For simplicity, these models did not directly consider nutrient limitation and instead used the logistic growth equation with a fixed carrying capacity to constrain the predator-free phytoplankton abundance, and subsequently explored how top-down control via predation and grazing affects the phytoplankton ability to bloom. Phytoplankton abundance is largely dependent on the bottom-up factors that affect growth, such as light intensity and the availability of a wide range of macro- and micro-nutrients [19]. In the mixed layer phytoplankton receive an equal amount of light, but they remove nutrients from the environment, making them unavailable to other cells [29, 19, 24, 26], including species at higher trophic levels. This important phenomenon is unexplained by previous models of the system.

Nutrient-Phytoplankton-Zooplankton (NPZ) models examine the quantities of nutrient and assimilated nutrient (plant and herbivore biomass) in a system and are a common tool used to model plankton interactions in the nutrient-limited marine environment [13, 29]. Here we construct an NPZ-style model with two species of zooplankton, microzooplankton and copepods, giving an NPMZ model which specifically includes infochemical-mediated interactions between trophic levels. After performing an asymptotic analysis on the existence and stability of equilibria, we study the behavior of the system under varying levels of infochemical-mediated predation (top-down control) and show it to produce results similar to those of earlier models. We then examine how the behavior of the system changes as the level of nutrient in the system (bottom-up control) is varied simultaneously. Finally we carry out a sensitivity analyses to determine the robustness of the model results. Importantly, we show the one-parameter bifurcation behavior of the top-down model to change when the total nutrient availability is changed, and hence demonstrate phytoplankton bloom formation to be a function of both top-down and bottom-up processes.

2. MULTITROPHIC FOOD-WEB MODEL

2.1. Full four-species model

The following meso-scale model describes interactions between small infochemical-producing phytoplankton, microzooplankton and copepods in a well-mixed system that is closed to nutrients. The state variables measure biomass in units of μg C l^{-1} for consistency with previous models [24, 26]. Under spring bloom conditions, the parameters are converted to the appropriate units using the conversion equivalences 1μg carbon $\equiv 20$ mg chlorophyll $\equiv 10$ mol nitrogen [8]. Dissolved nutrients (N) are assimilated by phytoplankton (P), which are then grazed by microzooplankton (M), thereby releasing chemicals into the surrounding environment. Microzooplankton are subject to predation from copepods (Z), which use the chemical information released following microzooplankton grazing on phytoplankton to increase the efficiency of their search. It is assumed any losses from the plankton are immediately returned to the dissolved nutrient pool ready for further uptake by phytoplankton. This assumption means that our model is valid over much longer time-scales than previous models of the system [i.e. a few days; 24, 26] as the nutrients released following the death of the plankton will go to higher trophic levels or take time to decay and remineralise [2]. This assumption of a closed system is made for simplicity and is common in many NPZ models, e.g. [2].

The model is given by:

$$\frac{dN}{dt} = -\frac{vNP}{k_0+N} + (1-\gamma)\frac{gPM}{k_1+P} + (1-\epsilon)\frac{\beta MZ}{k_2+M}\left(1+\frac{\xi gPM}{k_1+P}\right) + \mu M + \delta Z^2 \quad (1)$$

$$\frac{dP}{dt} = \frac{vNP}{k_0+N} - \frac{gPM}{k_1+P} \quad (2)$$

$$\frac{dM}{dt} = \frac{\gamma gPM}{k_1+P} - \mu M - \frac{\beta MZ}{k_2+M}\left(1+\frac{\xi gPM}{k_1+P}\right) \quad (3)$$

$$\frac{dZ}{dt} = \frac{\epsilon\beta MZ}{k_2+M}\left(1+\frac{\xi gPM}{k_1+P}\right) - \delta Z^2 \quad (4)$$

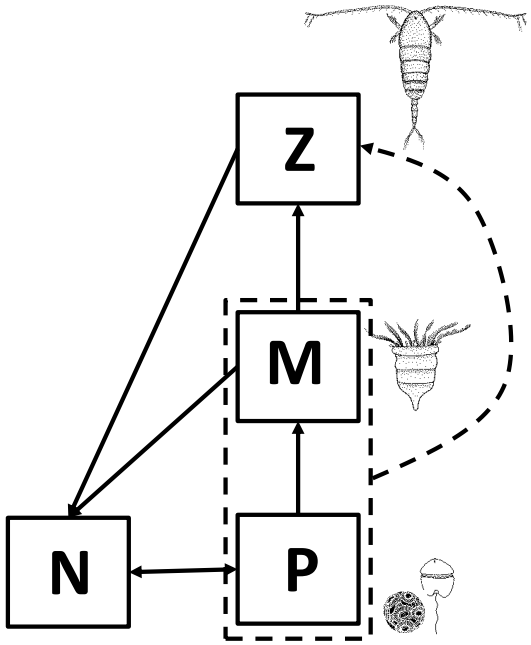

Figure 1: The interactions between nutrients (N), phytoplankton (P), microzooplankton (M) and copepods (Z) for the model given by Equations (1)–(4). As the total amount of nutrient in the system is fixed, the system reduces to Equations (7)–(9). Solid lines represent direct trophic interactions while the dashed line represents indirect chemical interactions.

where $N, P, M, Z \geq 0$ and all model parameters are non-negative and constant in time. In the model, phytoplankton assimilate dissolved nutrients according to the Michaelis-Menten functional response [29], with maximum uptake rate v and half saturation constant k_0. Under the assumption of a thoroughly mixed layer, phytoplankton receive an equal amount of light and therefore phytoplankton growth is limited by nutrient availability only. We assume microzooplankton and copepods follow Holling type II (Michaelis-Menten) functional responses [18] with maximum grazing/predation rates g and β, and half-saturation constants k_1 and k_2, respectively [24]. The copepod predation rate on microzooplankton is increased by a multiplicative factor $1 + (\xi g P M)/(k_1 + P)$, which represents an increase in copepod foraging efficiency through chemoreception proportional to the microzooplankton grazing rate on phytoplankton. The non-dimensional parameter ξ represents how an increase in the release of grazing-induced infochemicals corresponds to an increase in copepod predation [24, 25]. Microzooplankton convert grazed phytoplankton into new biomass with efficiency γ, while copepods convert predated microzooplankton into new biomass with efficiency ϵ. For simplicity, any losses from the plankton, either through mortality or unassimilated prey biomass, are returned immediately to the dissolved nutrient pool [e.g. 2]. These interactions are summarized in Figure 1.

2.2. Reduced three-species model

The assumption that any particulate nutrients stored in the plankton are immediately available as dissolved nutrients upon the death of the plankton means that the model equations follow the laws of conservation of mass and energy [2]. Hence, it follows that:

$$\frac{d}{dt}(N+P+M+Z)=0 \tag{5}$$

so that:

$$\frac{dN}{dt}=-\frac{dP}{dt}-\frac{dM}{dt}-\frac{dZ}{dt}\Rightarrow N(t)=T-P(t)-M(t)-Z(t) \tag{6}$$

where T is the constant of integration [3, 2], and represents the total amount of nutrient in the system, both particulate (incorporated in the plankton) and dissolved (available for uptake).

Because N is expressed in terms of P, M and Z (Equation (6)), Equations (1)–(4) can be rewritten as a system involving only P, M and Z:

$$\frac{dP}{dt} = \frac{vP(T-P-M-Z)}{k_0+T-P-M-Z}-\frac{gPM}{k_1+P} \tag{7}$$

$$\frac{dM}{dt} = \frac{\gamma gPM}{k_1+P}-\mu M-\frac{\beta MZ}{k_2+M}\left(1+\frac{\xi gPM}{k_1+P}\right) \tag{8}$$

$$\frac{dZ}{dt} = \frac{\epsilon\beta MZ}{k_2+M}\left(1+\frac{\xi gPM}{k_1+P}\right)-\delta Z^2 \tag{9}$$

with $T-P(t)-M(t)-Z(t)=N(t)\geq 0$ [3].

2.3. Parameter estimates

Based on the literature, the following parameter values are used in the model. The maximum nutrient uptake rate of phytoplankton is analogous to the maximum growth rate of logistic growth models, and belongs to the range $0.1<v<2\text{d}^{-1}$ [30]. The total amount of nutrients in the system is analogous to the carrying capacity term of logistic growth models. Franks [12] consider a phytoplankton carrying capacity of $T=50\mu\text{g C l}^{-1}$, whereas Morozov et al. [30] consider a much wider range of values (up to $T=\infty$). Edwards and Brindley [8] estimate the half saturation constant of phytoplankton to belong to the range $20<k_0<150\mu\text{g C l}^{-1}$. Infochemical producing phytoplankton, such as *Emiliania huxleyi* and *Phaeocstis* sp., are typically small, fast-growing and can rapidly form large blooms under favorable conditions [27]. Hence we parametrize using large values of v and T, and a small value of k_0. Microzooplankton growth rates are comparable to those of their phytoplankton prey, hence Edwards et al. [9] estimated that grazing must be of order $2<g<12\text{d}^{-1}$ to maintain rapid growth rates while accounting for the inefficiencies of converting phytoplankton into new biomass. The half saturation constants for both microzooplankton and copepods belong in the range $20<k_i<100\mu\text{g C l}^{-1}$ [8]. In our model, a low value of k_1 was chosen to reflect the rapid response of microzooplankton to favorable feeding conditions. Values of the maximum copepod predation rate and half saturation constant were chosen as $\beta=1\text{d}^{-1}$ and $k_2=30\mu\text{g C l}^{-1}$, in order to reflect that copepod dynamics evolve on slower time scales than microzooplankton dynamics [9, 10]. The microzooplankton conversion efficiency is estimated as $0.15<\gamma<0.64$ [37]. Kiørboe [20] states that the conversion efficiency may be higher when considering copepods feeding on microzooplankton, hence a higher value of $\epsilon=0.7$ is chosen for the copepod assimilation efficiency. This is in agreement with the values used by Edwards et al. [9, 10] to study microzooplankton and copepod dominated systems respectively. Zooplankton mortality rates belong to the range $0.015<\mu,\delta<0.15\text{d}^{-1}$ [8]. In our model, copepods are parametrized with a larger mortality value to account for predation from higher predators as well as natural mortality; microzoplankton suffer a smaller natural mortality as it is assumed most predation is from copepods, which are modelled explicitly. The parameter ξ is here considered a control/bifurcation parameter which will be varied to consider the effect of infochemical-mediated predation on the system. These parameter values are summarized in Table 1.

Table 1: Parameter values for Equations (7)–(9). Parameters are fixed at the default value unless otherwise stated.

Parameter	Definition	Units	Default Value	Range
T	Total nutrients (particulate + dissolved)	μg C l^{-1}	120	$50 - \infty$
v	Maximum nutrient uptake rate	d^{-1}	1.5	$0.1 - 2$
g	Maximum microzooplankton grazing rate	d^{-1}	6	$2 - 12$
β	Maximum copepod predation rate	d^{-1}	1	$0.6 - 1.4$
k_0	Half saturation constant	μg C l^{-1}	20	$20 - 150$
k_1	Half saturation constant	μg C l^{-1}	20	$20 - 100$
k_2	Half saturation constant	μg C l^{-1}	35	$20 - 100$
γ	Microzooplankton grazing efficiency	–	0.3	$0.15 - 0.64$
ϵ	Copepod predation efficiency	–	0.7	$0.3 - 0.7$
μ	Microzooplankton natural mortality	d^{-1}	0.1	$0.015 - 0.15$
δ	Copepod mortality	d^{-1}	0.15	$0.015 - 0.15$
ξ	Infochemical-mediated predation	–	Control parameter	–

3. ASYMPTOTIC ANALYSIS ON THE EXISTENCE AND STABILITY OF EQUILIBRIA

A mathematical understanding of the system described by Equations (7)–(9) is obtained by considering the existence and stability of its equilibria. Firstly, we note that from (9) the copepod equilibrium, Z_e, is given by

$$Z_e = 0, \quad \text{and} \quad Z_e = \frac{\epsilon\beta M_e \left(k_1 + P_e \left(1 + \xi g M_e\right)\right)}{\delta \left(k_1 + P_e\right)\left(k_2 + M_e\right)}. \tag{10}$$

We now consider the existence and stability of the system equilibria, (P_e, M_e, Z_e), for these two different values of Z_e. Writing $(P, M, Z) = (P_e, M_e, Z_e) + \varepsilon e^{\lambda t}(p, m, z)$, $|\varepsilon| \ll 1$, substituting into the governing equations, and taking the linear order of the expansions in ε gives an eigenvalue problem; an equilibrium is stable when the real part of λ is negative.

3.1. Trivial equilibria (with $Z_e = 0$)

Considering $Z_e = 0$, we obtain three trivial equilibria: two non-hyperbolic and one hyperbolic (Table 2). We consider each equilibrium in more detail below.

1) ***Extinction equlibrium point****:* The extinction equilibrium point at $(P_e, M_e, Z_e) = (0, 0, 0)$ corresponds to the extinction of all plankton species. Simple calculations give the Jacobian

$$J = \begin{pmatrix} vT/(k_0 + T) & 0 & 0 \\ 0 & -\mu & 0 \\ 0 & 0 & 0 \end{pmatrix}, \tag{11}$$

from which we obtain the eigenvalues of the linearisation operator about the state:

$$\lambda = vT/(k_0 + T),\ -\mu,\ 0. \tag{12}$$

A corresponding eigenvector of the zero eigenvalue is

$$\underline{u} = (0, 0, 1). \tag{13}$$

It is then interesting to know the type of the nonhyperbolic equilibrium along the direction of the zero eigenvalue. Here, we will use a formal expansion by setting the nonhyperbolic direction to be slowly varying in t, i.e. we write

$$(P, M, Z) = \varepsilon a(\hat{t})\underline{u} + \varepsilon^2(\tilde{p}(t), \tilde{m}(t), \tilde{z}(t)),\ \hat{t} = \varepsilon t. \tag{14}$$

Substituting this into the governing equation and linearising about $\varepsilon = 0$ gives a set of differential equations. The first non-zero terms are at $\mathcal{O}(\varepsilon^2)$, which are given by

$$\begin{pmatrix} \dot{\tilde{p}}(t) \\ \dot{\tilde{m}}(t) \\ \dot{\tilde{z}}(t) \end{pmatrix} = J \begin{pmatrix} \tilde{p}(t) \\ \tilde{m}(t) \\ \tilde{z}(t) \end{pmatrix} + \begin{pmatrix} 0 \\ 0 \\ -\frac{da}{d\hat{t}} - \delta a(\hat{t})^2 \end{pmatrix}. \tag{15}$$

Without the second term on the right hand side, the equations above are nothing else, but the eigenvalue problem for the extinction equilibrium point. Requiring the asymptotic expansion above to be uniform yields the following dynamics for a

$$\frac{da}{d\hat{t}} = -\delta a(\hat{t})^2. \tag{16}$$

Hence, the zero eigenvalue corresponds to a stable manifold. Therefore, for all parameter values, the extinction equilibrium is an unstable saddle point.

2) ***Phytoplankton only equilibrium point****:* The phytoplankton only equilibrium point at $(P_e, M_e, Z_e) = (T, 0, 0)$ corresponds to the extinction of microzooplankton and copepods. In the absence of predation from higher trophic levels, phytoplankton are able to assimilate all available nutrients and survive at the total carrying capacity of the system, T. The eigenvalues are given by:

$$\lambda = -vT/k_0,\ \gamma g T/(k_1 + T) - \mu,\ 0. \tag{17}$$

Performing the same computations as those for extinction equilibrium, yields the same result that the zero eigenvalue corresponds to a stable manifold. Therefore the stability of the phytoplankton only equilibrium depends of the sign of the second eigenvalue. When $\gamma g T/(k_1 + T) < \mu$ this eigenvalue has negative real part and the equilibrium point is stable; otherwise, the equilibrium point is an unstable saddle point. For the default parameter values in Table 1, we have the phytoplankton only equilibrium is an unstable saddle point.

3) ***Copepod-free equilibrium point****:* The copepod-free equilibrium point at $(P_e, M_e, 0)$ corresponds to the extinction of copepods only and, in the absence of predation, allows microzooplankton to control the phytoplankton population. Here

$$P_e = \frac{\mu k_1}{\gamma g - \mu}, \tag{18}$$

and M_e satisfies the quadratic equation

$$g M_e^2 - (v(k_1 + P_e) + g(k_0 + T - P_e))\, M_e + v(T(k_1 + TP_e) - P_e(k_1 + P_e)) = 0, \tag{19}$$

which can be solved analytically. However, when we use the simple expressions of the equilibria directly, the corresponding eigenvalues have lengthy expressions, which are almost impossible to analyse. In order to make analytic progress we use an asymptotic scaling. Based on the parameter values in Table 1, we choose the following scaling

$$T = \widehat{T}/\mu^2,\ k_j = \mu\widehat{k}_j,\ \delta = \mu\widehat{\delta}, \epsilon = \mu\widehat{\epsilon},\ \gamma = \mu\widehat{\gamma},\ \xi = \mu\widehat{\xi}, \tag{20}$$

where $0 < \mu \ll 1$ and the other parameters are of $\mathcal{O}(1)$. Using this scaling, the copepod-free equilibrium becomes

$$(P_e, M_e) = \left(\frac{\widehat{k}_1}{(\widehat{\gamma} g - 1)\,\mu} + \mathcal{O}(1), \frac{\widehat{T}}{\mu^2} + \mathcal{O}(\mu^{-1}) \right) \tag{21}$$

and

$$(P_e, M_e) = \left(\frac{\widehat{k}_1}{(\widehat{\gamma} g - 1)\,\mu} + \mathcal{O}(1), \frac{v\widehat{k}_1\widehat{\gamma}}{(\widehat{\gamma} g - 1)\,\mu} + \mathcal{O}(1) \right). \tag{22}$$

Note that only the equilibrium given in (22) is biologically relevant, as (21) gives $N = T - P_e - M_e - Z_e = -\widehat{k}_1/(\widehat{\gamma}\mu g - \mu) + \mathcal{O}(1)$, i.e. it violates the condition that $N(t) \geq 0$. For the parameter values in Table 1 it is straightforward to show that the copepod-free equilibrium is hyperbolic. One of the eigenvalues is given by

$$\lambda = \frac{\mu(\widehat{\xi}\widehat{k}_1 v + \widehat{\gamma}g - 1)\widehat{\gamma}^2\widehat{k}_1 v\beta\widehat{\epsilon}}{\widehat{\gamma}(\widehat{\gamma}v\widehat{k}_1 + (\widehat{\gamma}g - 1)\widehat{k}_2)(\widehat{\gamma}g - 1)} + \mathcal{O}(\mu^2).$$

The other eigenvalues are generally a complex conjugate pair that satisfy the quadratic equation

$$\left(\lambda - \frac{d}{dP}\left(\frac{dP}{dt}\right)\right)\left(\lambda - \frac{d}{dM}\left(\frac{dM}{dt}\right)\right) - \frac{d}{dM}\left(\frac{dP}{dt}\right)\frac{d}{dP}\left(\frac{dM}{dt}\right) = 0$$

at $P = P_e$, $M = M_e$, and $Z = 0$. Because the Routh-Hurwitz conditions of the characteristic polynomial fail to hold, the equilibrium is unstable.

3.2. Coexistence equilibria (with $Z_e \neq 0$)

*1) **Location of coexistence equlibria**:* Next, we consider the coexistence states, where Z_e in (10) is non-zero. We continue with the earlier choice of scaling (20). Based on numerical simulations, we use the scaling

$$P = P_0/\mu^2 + \ldots,\ M = M_0/\mu + \ldots, \tag{23}$$

and consequently $Z = Z_0 + \ldots$. Substituting these expansions into (7) and (8), we find that

$$P_0 = \widehat{T}, \tag{24}$$

and M_0 satisfies the polynomial equation

$$-\left(\beta\widehat{\xi}g\right)^2\widehat{\epsilon}M_0^3 + \left(\widehat{\delta}\widehat{\gamma}g - 2\widehat{\epsilon}\widehat{\xi}g\beta^2 - \widehat{\beta}^2\right)M_0^2 + \left(2\widehat{\delta}\widehat{k}_2\left(\widehat{\gamma}g - 1\right) - \widehat{\epsilon}\beta^2\right)M_0 + \widehat{\delta}\widehat{k}_2^2\left(\widehat{\gamma}g - 1\right) = 0, \tag{25}$$

which can be solved explicitly as it is just a quadratic equation in $\widehat{\xi}$. Analyzing the root numerically using parameter values given in the table, we conclude that only one of the roots is acceptable as the other one corresponds to negative $\widehat{\xi}$.

In addition to the scaling (23), again based on numerical observations one could also choose to take the scaling

$$P = P_0/\mu + \ldots,\ M = M_0/\mu + \ldots, \tag{26}$$

which at leading order then yields

$$P_0 = \left(gM_0 - v\widehat{k}_1\right)/v, \tag{27}$$

and M_0 satisfies the polynomial equation

$$\sum_{n=0}^{4} a_n M_0^n = 0, \tag{28}$$

with

$$a_4 = \left(\beta\widehat{\xi}g\right)^2\widehat{\epsilon},\ a_3 = -2\widehat{\epsilon}\widehat{\xi}g\left(v\widehat{k}_1\widehat{\xi} - 1\right)\beta^2 - \widehat{\delta}(\widehat{\gamma}g - 1),$$
$$a_2 = \widehat{\epsilon}(v\widehat{k}_1\widehat{\xi} - 1)^2\beta^2 + \widehat{\delta}(2\widehat{k}_2(1 - \widehat{\gamma}g) + \widehat{\gamma}\widehat{k}_1 v),$$
$$a_1 = 2\widehat{\delta}\widehat{\gamma}\widehat{k}_1\widehat{k}_2 v - \widehat{\delta}(\widehat{\gamma}g - 1)\widehat{k}_2^2,\ a_0 = \widehat{\gamma}\widehat{\delta}\widehat{k}_1\widehat{k}_2^2 v,$$

which again is a quadratic equation in $\widehat{\xi}$ and hence can be solved explicitly.
Note that for the scaling and results (23)-(25) and (26)-(28), the corresponding value Z are given by the second expression in (10).

Shown in Fig. 2 are plots of the scaled variables P_0, M_0, and Z_0 using the default parameter values given in Table 1.

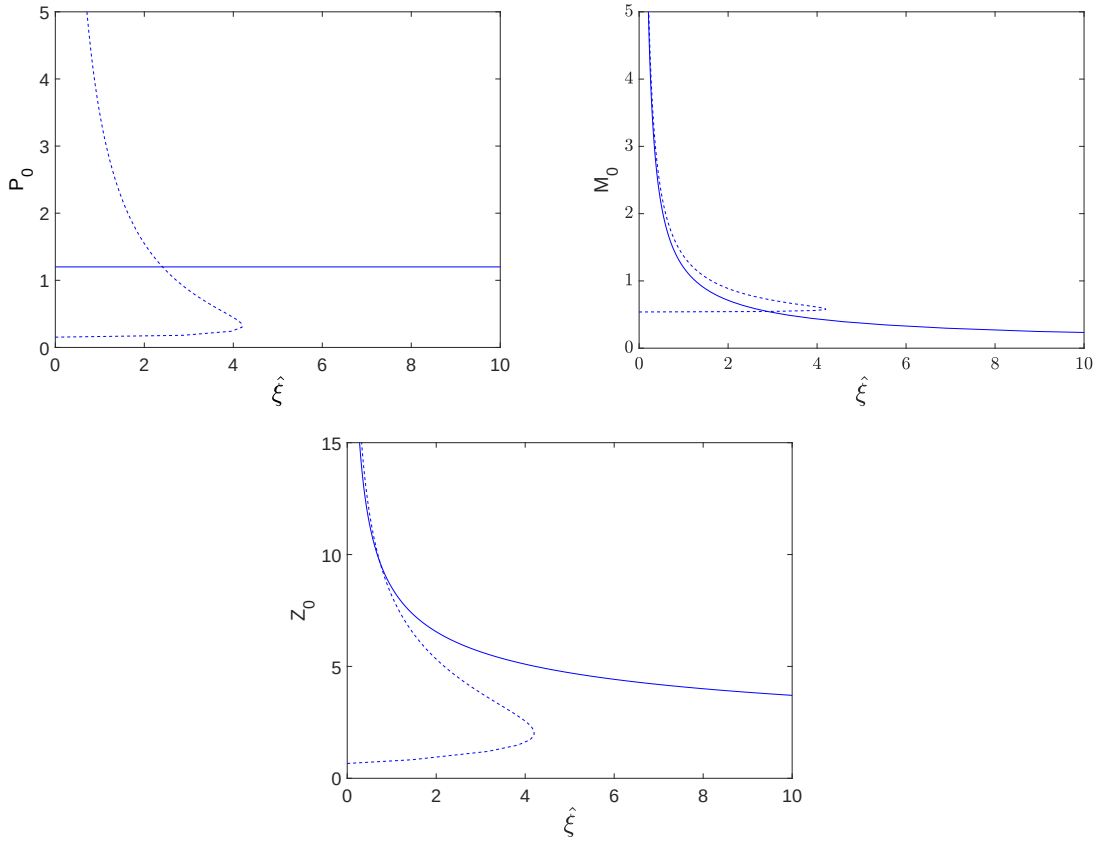

Figure 2: Plots of (24)-(25) and (27)-(28) and their corresponding Z_e (10) showing the asymptotic behavior of the bifurcation curves as $\mu \to 0$. The solid and dashed lines show the curve obtained from scaling (23) and (26), respectively, together with the scaling (20).

2) ***Stability of coexistence equilibria****:* Next, we would like to determine the stability of the coexistence states by computing the eigenvalues of the linearisation operator about the equilibrium states asymptotically. However, despite the simple expressions of the equilibrium using the scaling (23) and (26), the corresponding characteristic polynomials of the stability matrix are too cumbersome. With the help of MAPLE [28], we obtain the leading order behaviour of the polynomial coefficients that are given by

$$\lambda^3 + \mathcal{O}(\mu^{-1})\lambda^2 + \mathcal{O}(\mu^{-2})\lambda + \mathcal{O}(\mu) = 0, \tag{29}$$

$$\lambda^3 + \mathcal{O}(1)\lambda^2 + \mathcal{O}(\mu^{-2})\lambda + \mathcal{O}(\mu^2) = 0, \tag{30}$$

for the scaling (23) and (26), respectively, where λ is again the spectral parameter and the equilibrium state is stable when $\mathrm{Re}(\lambda) < 0$.

Theoretically, the characteristic equations above can be solved analytically. Yet, due to the complicated expressions of the coefficients in the polynomials, we have to rely on numerical computations, from which we obtain that for the parameter values given in the table, all the coexistence states are generally hyperbolic, namely the eigenvalues are non-zero.

3.3. Summary of the asymptotic analysis of equilibria

We have shown that the system potentially has (at least) five biologically relevant equilibria: the non-hyperbolic extinction state $(P_e, M_e, Z_e) = (0, 0, 0)$, the non-hyperbolic phytoplankton only state $(P_e, M_e, Z_e) =$

Table 2: Biologically relevant equilibria of the system given by Equations (7)–(9) and evaluated for the default parameter values given in Table 1.

Equilibrium	Definition	Value in parametrized system	Description	Type
E_0	$(0,0,0)$	$(0,0,0)$	Extinction equilibrium	Non-hyperbolic
E_1	$(P_e,0,0)$	$(120,0,0)$	Phytoplankton only equilibrium	Non-hyperbolic
E_2	$(P_e,M_e,0)$	$(1.176,4.506,0)$	Copepod-free equilibrium	Hyperbolic
E_3	(P_e,M_e,Z_e)	Depends on ξ	Coexistence equilibrium	Hyperbolic

$(T,0,0)$, two potential copepod-free equilibria given by Equations (21) and (22), and the full co-existence persistence state. Further coexistence equilibria may exist for parameter values outside the range where the asymptotic analysis is valid, as we will show numerically in the next section.

We have demonstrated that the zero eigenvalues of the non-hyperbolic equilibria correspond to stable manifolds, and that these equilibria are unstable saddles for the default parameter values given in Table 1. In addition, for the parameter values given in Table 1, the latter three equilibria are all hyperbolic, but the second copepod-free state given by Equation (22) does not satisfy the condition that $T - P(t) - M(t) - Z(t) = N(t) \geq 0$. The resulting four biologically relevant equilibria are summarised in Table 2.

4. NUMERICAL ANALYSIS AND SIMULATIONS

Next, we present numerical computations of the governing equations (7)–(9) to both verify and illustrate the asymptotic analysis in Section 3, and also to explore the system dynamics in more detail within a reasonable range of parameter values. In Section 4.1 we present phase portraits and trajectories of the state variables when all parameters are set to their default values in Table 1 and show the dynamics to change when infochemical-mediated predation (ξ) is included. In Section 4.2 we construct one-parameter bifurcation diagrams demonstrating how this qualitative change occurs as ξ is increased. In Section 4.3 we construct two-parameter bifurcation diagrams to explore how the one-parameter bifurcation behaviour changes as the level of nutrient (T) in the system is varied simultaneously. Finally, in Section 4.4, we carry out a sensitivity analyses by varying each model parameter simultaneously with ξ.

4.1. Phase portraits and numerical simulations

Figure 3 shows the phase portrait and time series plot for when $\xi = 0$, starting from initial conditions chosen arbitrarily as $(P,M,Z) = (60,10,5)$, and with all parameters fixed at their default values in Table 1. It can be seen from Figure 3 that the trajectories converge to a stable limit cycle, where the phytoplankton population blooms periodically over time. Solving Equations (7)–(9) numerically for $\xi = 0$ shows this coexistence equilibrium to be a unique saddle-focus at $E_3 = (1.347, 4.538, 0.536)$. Trajectories will spiral away from this point to the stable limit cycle. The copepod-free equilibrium (E_2) is an unstable focus-node and hence trajectories will never tend to this point when $\xi = 0$. Section 3 shows the two non-hyperbolic equilibria to be unstable saddles for the default parameter values. Hence the limit cycle surrounding the persistence equilibrium at $E_3 = (1.347, 4.538, 0.536)$ must be globally attracting.

Figure 4 shows a phase portrait and time series plot for when ξ is 0.2, keeping the same initial conditions and all other parameters fixed at the default values in Table 1. It can be seen that including infochemical-mediated predation causes the system to undergo a qualitative change, where trajectories now converge to a stable steady state (Figure 4b). This steady state corresponds to a sustained phytoplankton bloom (a high level of P is maintained indefinitely). Solving Equations (7)–(9) numerically for $\xi = 0.2$ reveals this solution to be a stable focus-node at $E_{3B} = (98.734, 7.505, 6.994)$. Solving Equations (7)–(9) numerically also reveals the existence of two further coexistence equilibria at $E_{3L} = (1.507, 4.569, 0.746)$ and $E_{3U} = (22.099, 8.493, 5.787)$, both of which are unstable saddle-foci with negative- and positive- real eigenvalues respectively.

The stabilities of the trivial equilibria ($E_0 - E_2$) remain unchanged from when $\xi = 0$, and therefore repel trajectories. These results suggest two locally attracting persistence states in the phase space; a limit cycle surrounding the unstable saddle-focus at $E_{3L} = (1.507, 4.569, 0.746)$ and a stable focus-node at $E_{3B} = (98.734, 7.505, 6.994)$, a trajectory of which is shown in Figure 4.

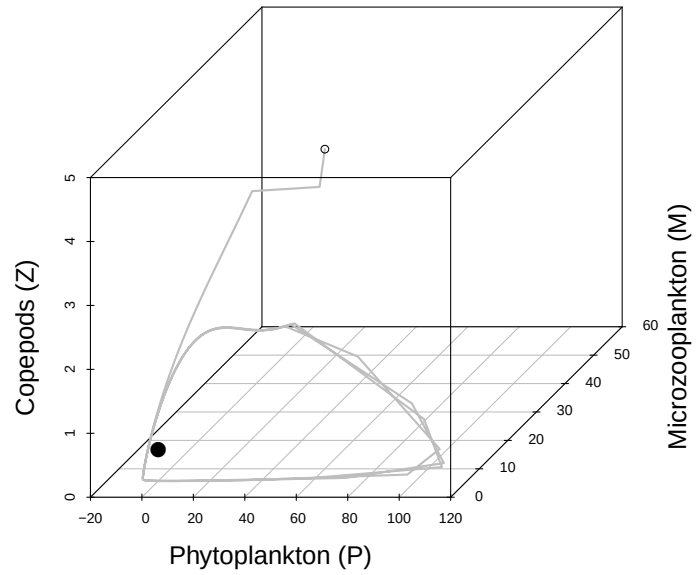

(a)

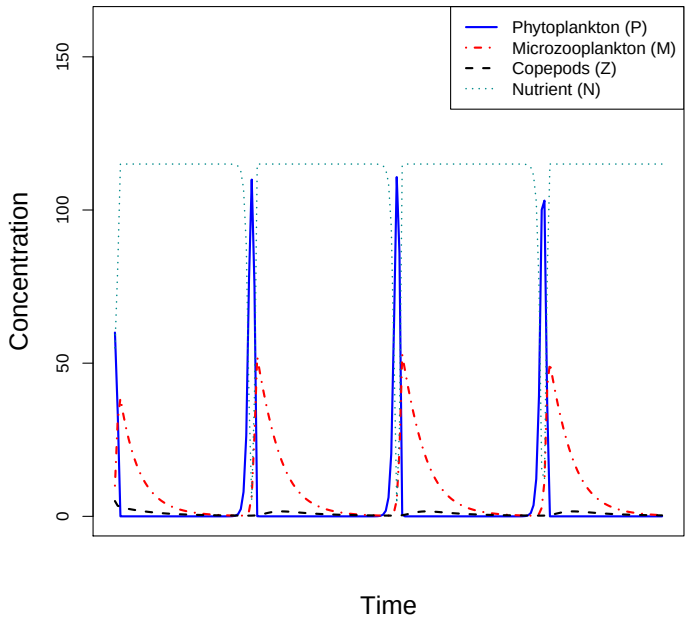

(b)

Figure 3: Phase portrait and time series of P, M, Z and N for $\xi = 0$ and with all other parameters fixed at the default values given in Table 1. Solutions tend to a stable limit cycle around E_3 corresponding to the coexistence of all plankton species. Figures generated using deSolve in R [34].

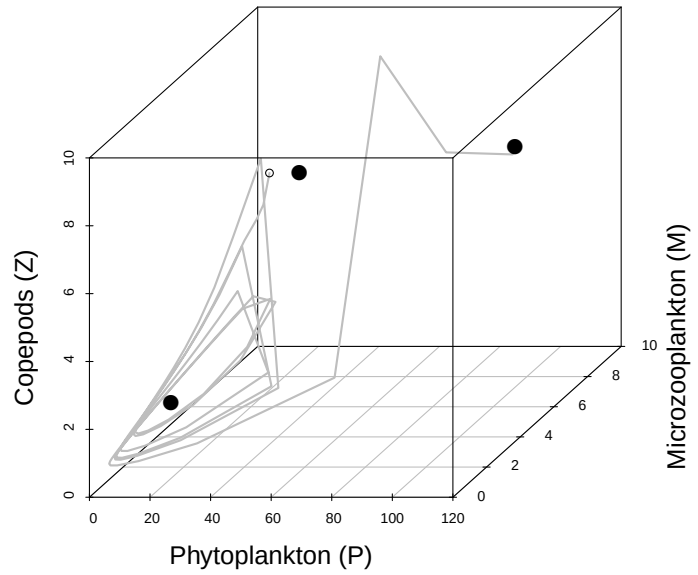

(a)

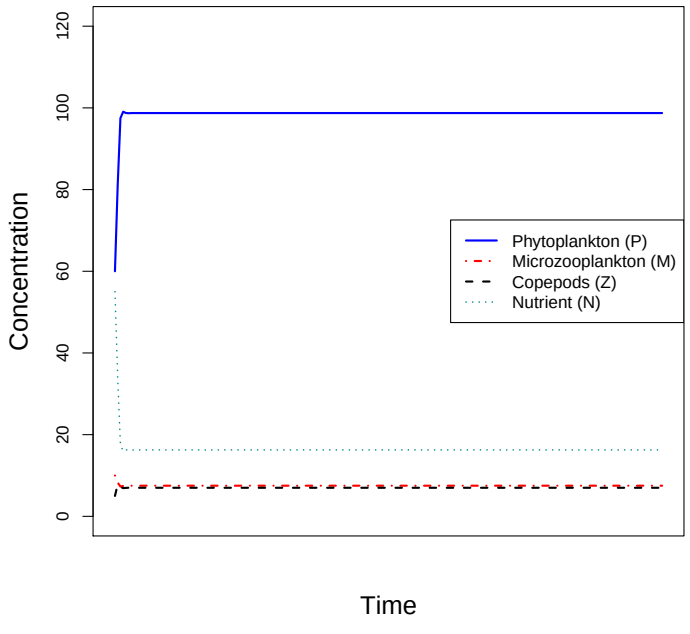

(b)

Figure 4: A phase portrait and time series trajectory when $\xi = 0.2$ and all other parameters are fixed at the values given in Table 1. Solutions tend to a locally stable steady state corresponding to the persistence of all plankton species (E_{3B}). Figures generated using deSolve in R [34].

4.2. One-parameter bifurcation analysis

The qualitative difference between Figures 3 and 4 indicates that there has been a bifurcation between $0 < \xi < 0.2$. Figure 5 gives bifurcation diagrams for which ξ is varied continuously, and shows the exact values of ξ where bifurcations occur as well as the steady state concentrations of P, M and Z and their limit cycle ranges.

Figure 5a shows the equilibrium concentration(s) of P as ξ is varied continuously. For $\xi < 0.494$ there exists a saddle-focus coexistence equilibrium (E_{3L} in Figure 5a); trajectories spiral away from this point to a stable limit cycle, the range of which is shown by the dot-dashed line in Figure 5a. A supercritical Hopf bifurcation at $\xi = 0.494$ (H in Figure 5a) destroys this limit cycle and causes the saddle-focus to stabilize. Two saddle-node bifurcations at $\xi = 0.114$ and $\xi = 0.556$ (LP_1 and LP_2 in Figure 5a) create a region of bistability; the lower branch (E_{3L} in Figure 5a) corresponds to either a saddle-focus ($\xi <$ H) or a stable focus-node ($\xi >$ H) and the upper branch (E_{3B} in Figure 5a) is a stable focus-node corresponding to a phytoplankton bloom, a simulation of which is shown in Figure 4. From $\xi = 0.556$ there exists just one globally stable focus-node (E_{3B} in Figure 5a) corresponding to high concentrations of phytoplankton. In this situation, increased copepod predation on microzooplankton releases grazing pressure on phytoplankton and allows the formation of a phytoplankton bloom that is sustained indefinitely over time.

Figures 5b and 5c are the equivalent bifurcation diagrams showing the equilibrium concentrations of M and Z. From Figure 5b it can be seen that the branch prior to the saddle-node bifurcation at $\xi = 0.556$ (right LP in Figure 5b) corresponds to a fairly constant concentration of microzooplankton. The branch following the saddle-node bifurcation at $\xi = 0.114$ (left LP in Figure 5b) shows the equilibrium concentration of M to decrease with increasing ξ. In this situation a higher value of ξ results in a higher copepod predation rate on microzooplankton, and therefore, an increase in microzooplankton mortality.

From Figure 5c, the branch prior to the saddle-node bifurcation at $\xi = 0.556$ (right LP in Figure 5c) shows the equilibrium concentration of Z to increase with increasing ξ, as would be expected when copepods increase their predation rate in response to chemical cues. However, the branch following the saddle-node bifurcation at $\xi = 0.114$ (left LP in Figure 5c) shows the equilibrium concentration of Z to decrease with increasing ξ. This is a counterintuitive result, as copepod concentrations should be expected to increase with increasing predation rates. An explanation is that the steady state copepod concentration decreases with that of its prey because there is less biomass available to sustain the copepod population, as was observed in [26]. This decrease in M and Z biomass concentrations, subsequently allows P to reach higher concentration levels for the same total available nutrients, T.

Comparing Figure 5 to Figure 2, it can be seen that the predicted asymptotic behavior of the bifurcation curves agrees with the numerical results as $\mu \to 0$ ($T \to \infty$).

4.3. Two-parameter bifurcation analysis

Figure 6 shows how the one-parameter bifurcation behavior of the system changes as the total nutrient, T, is varied continuously with infochemical-mediated predation, ξ. When T is varied within the range specified in Table 1 ($50 \leq T\mu$g C $l^{-1} \leq 120$) the bifurcation behaviour described in Section 4.2 undergoes no qualitative change. However, varying the total nutrient, T, slightly below this range results in three further qualitatively different types of bifurcation behaviour.

Decreasing the total nutrient from the value of 120μg C l^{-1} in Table 1 causes the first saddle-node curve and the Hopf curve (LP and H in Figure 6) to swap positions at T_1, following which the Hopf bifurcation occurs before the first saddle-node bifurcation as ξ is increased from zero. In this situation it is still possible for phytoplankton to bloom (dark gray area in Figure 6) but a higher infochemical-mediated predation value is required.

Further decreasing the total nutrient results in a Cusp bifurcation at $T_2 = 22.6\mu$g C l^{-1}, $\xi = 1.64$ (CP in Figure 6), where the two saddle-node bifurcation curves (LPs in Figure 6) collide and disappear. Following the Cusp bifurcation, the initially unstable system (light gray area in Figure 6) stabilizes as ξ crosses the Hopf bifurcation curve (H in Figure 6). Following the Cusp bifurcation, that is for $T < 22.6\mu$g C l^{-1}, it is impossible for a phytoplankton bloom to form.

Decreasing the total nutrient to T_3 (Figure 6) causes the Hopf bifurcation curve to disappear, following which the system undergoes no bifurcations as ξ is increased from zero. In this situation there exists a

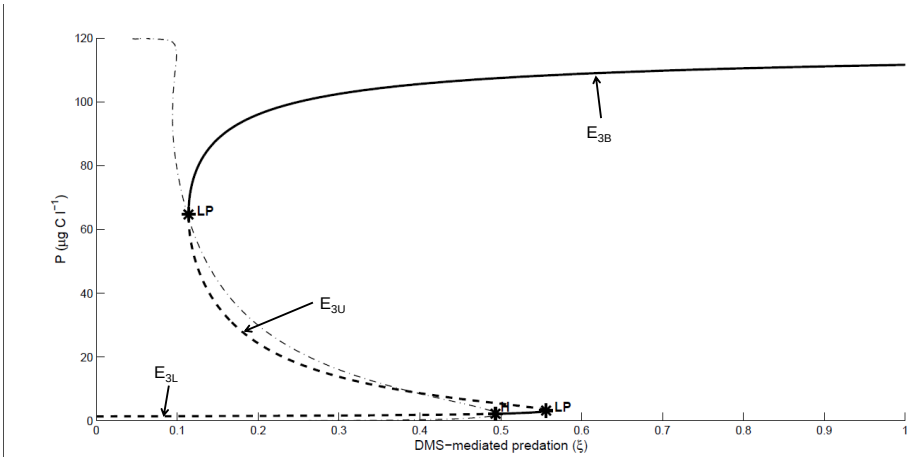

(a)

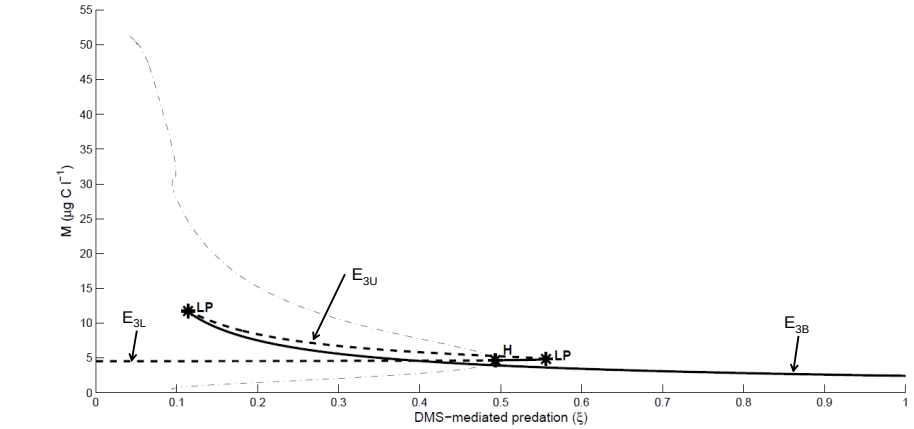

(b)

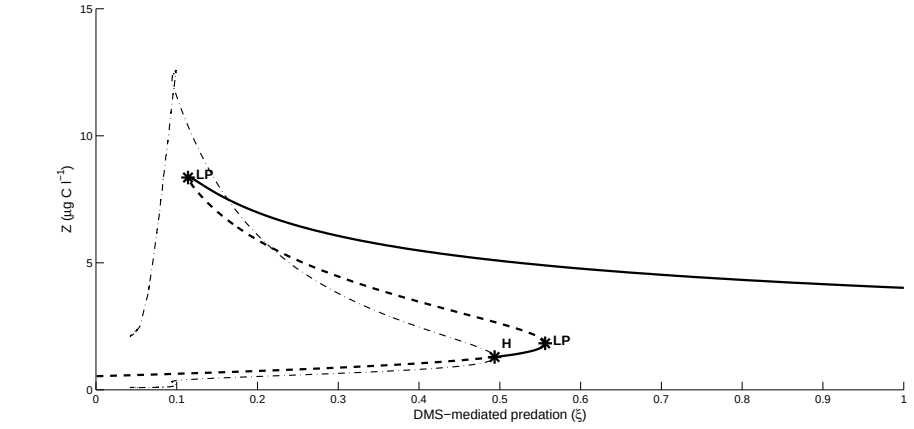

(c)

Figure 5: Bifurcation diagrams for variation of ξ, showing the equilibrium concentrations of **(a)** Phytoplankton (P), **(b)** Microzooplankton (M) and **(c)** Copepods (Z). The dashed-solid line shows where the equilibria occur as ξ is increased, with the dashed sections representing unstable equilibria and the solid sections representing stable equilibria. Stars represent bifurcation points and the dot-dashed line shows the magnitude of the limit cycle for a negligible infochemical effect. H=Hopf; LP=Limit point (saddle-node bifurcation). Plots generated numerically using MATCONT [5].

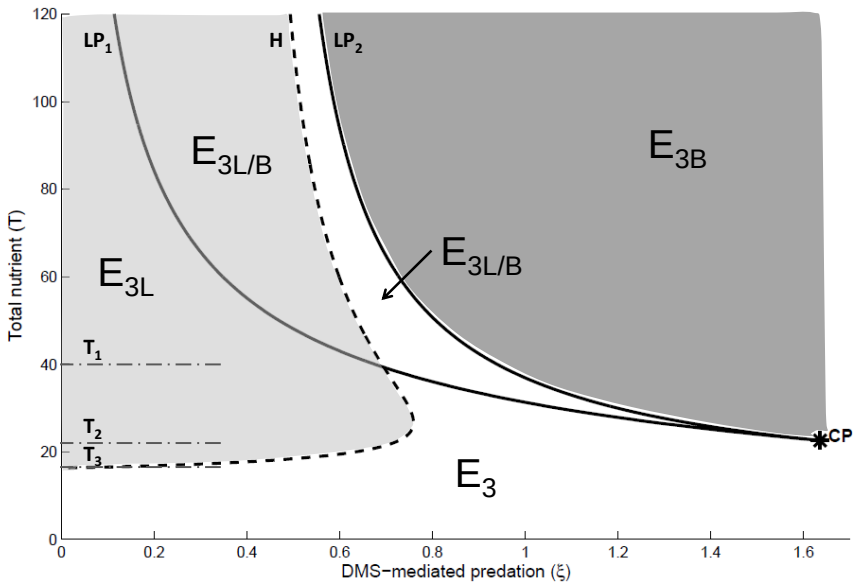

Figure 6: Two parameter bifurcation diagram for variation of ξ and T. The solid line shows the position of the saddle-node bifurcations while the dashed line shows the position of the Hopf bifurcation. Unstable regions are shaded light gray and regions where phytoplankton bloom formation always occur are shaded dark gray. Where bistability is possible, E_{3L} indicates where solutions converge to a stable limit cycle at low phytoplankton abundance while E_{3B} indicates where solutions converge to the stable phytoplankton bloom equilibrium. CP = Cusp (at $\xi = 1.64, T = 22.6$). Plot generated numerically using MATCONT [5].

permanently stable coexistence equilibrium (E_3 in Figure 6) where phytoplankton are unable to bloom, and all species are maintained at low biomass concentrations.

Figure 6 shows that decreasing the value of T in the model acts to shift the position of the saddle-node bifurcations (solid lines in Figure 6) to higher values of ξ, meaning that in nutrient deplete areas a higher infochemical-mediated predation value is required to create enough of a grazing refuge for phytoplankton to bloom. Furthermore, when $T < 22.6\mu$g C l^{-1} phytoplankton are unable to assimilate enough nutrients to reach bloom forming concentrations, making phytoplankton bloom formation impossible regardless of the value of ξ (infochemical-mediated predation).

4.4. Sensitivity analyses

The Cusp bifurcation in Figure 6 qualitatively changes the one-parameter bifurcation behaviour of the system. Here similar two-parameter bifurcation analyzes are carried out to assess how the one-parameter bifurcation behaviour of the system changes as each of the other parameters in the model is varied independently across its range in Table 1. This acts as a sensitivity analyses to test the robustness of model results within reasonable parameter ranges, where the lack of further codim-2 bifurcations suggests a higher level of model robustness. Results of this analysis are given in Figure 7.

Figure 7 shows that, except for the microzooplankton grazing rate (g; Figure 7b) and copepod mortality rate (δ; Figure 7j) no codim-2 bifurcations occur as the other parameters are varied with infochemical-mediated predation, ξ. Therefore, variation of these parameters within their reported ranges (Table 1) will not qualitatively alter the shape of the one-parameter bifurcation diagrams given in Figure 5. Increasing the nutrient uptake rate, v, copepod predation rate, β, microzooplankton half-saturation constant, k_1, copepod

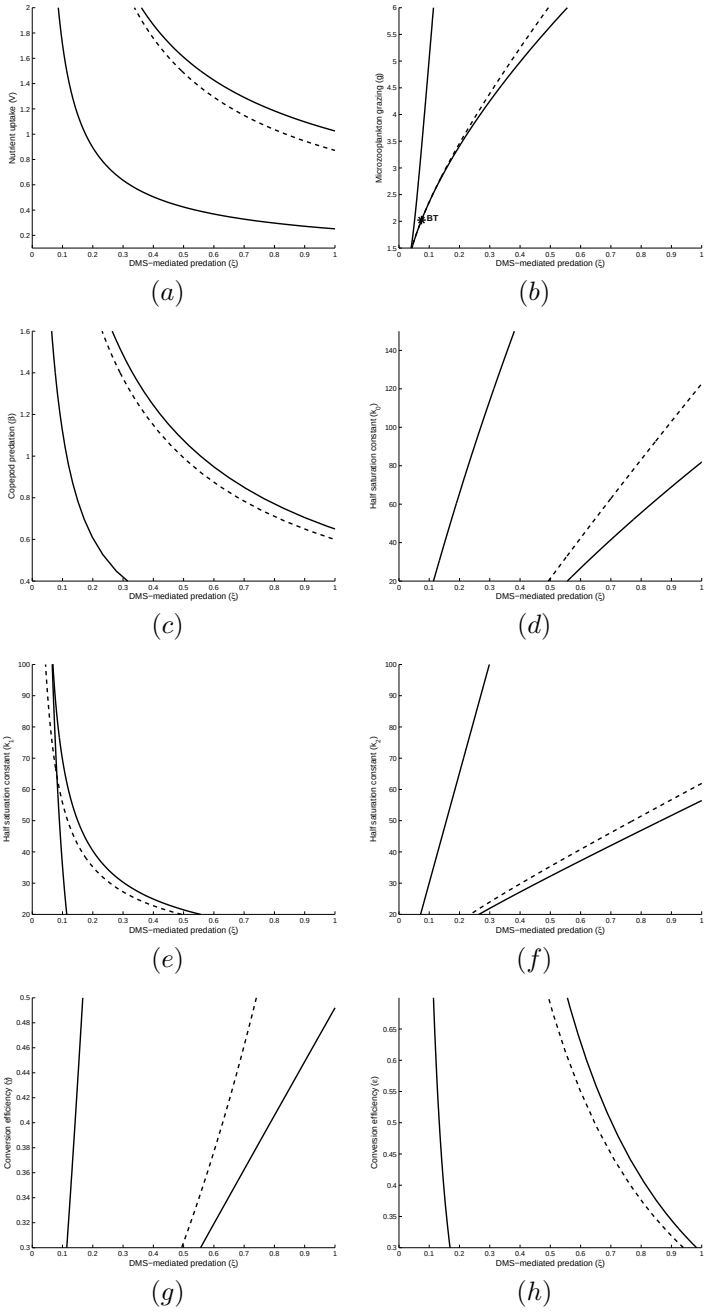
Nutrient uptake (V)
DMS−mediated predation (ξ)
(a)
Microzooplankton grazing (ĝ)
BT
DMS−mediated predation (ξ)
(b)
Copepod predation (β̂)
DMS−mediated predation (ξ)
(c)
Half saturation constant (k1)
DMS−mediated predation (ξ)
(d)
Half saturation constant (k1)
DMS−mediated predation (ξ)
(e)
Half saturation constant (k2)
DMS−mediated predation (ξ)
(f)
Conversion efficiency (ĝ)
DMS−mediated predation (ξ)
(g)
Conversion efficiency (ε)
DMS−mediated predation (ξ)
(h)

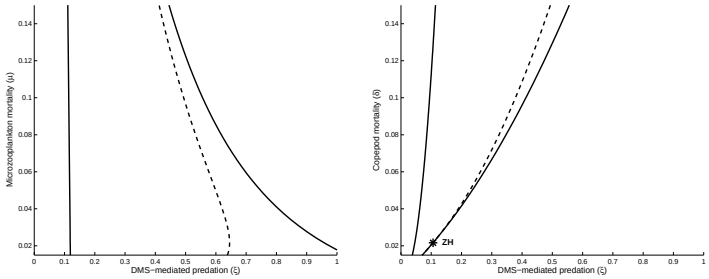

(i) (j)

Figure 7: Two parameter bifurcation diagrams for variation ξ with each of the other parameters, varied independently within the ranges reported in Table 1. The parameters not being varied are fixed at the values given in Table 1. The black lines show the position of the saddle-node bifurcations, dashed lines the position of the Hopf bifurcation. BT = Bogdanov-Takens (at $\xi = 0.075, g = 2.204$ in Figure b); ZH = Zero-Hopf (at $\xi = 0.106, \delta = 0.022$ in Figure j). Plots generated numerically using MATCONT [5].

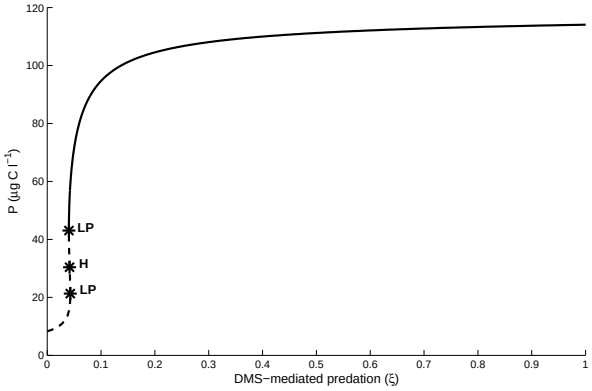

(a)

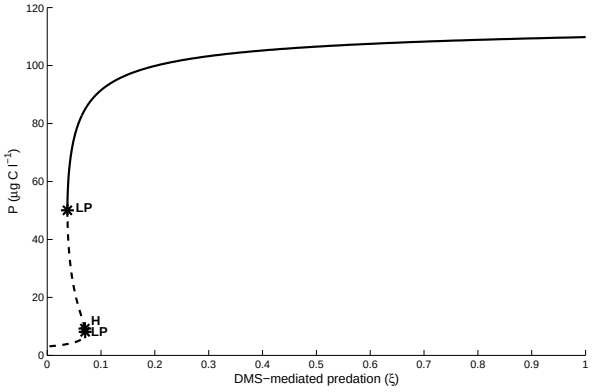

(b)

Figure 8: Bifurcation diagrams for variation of ξ after **(a)** g has been decreased through the Bogdanov-Takens bifurcation point ($g = 1.5$) and **(b)** δ has been decreased through the zero-Hopf bifurcation point ($\delta = 0.015$). H = neutral saddle in **(a)**, Hopf in **(b)**; LP = limit point (saddle-node bifurcation). Plots generated numerically using MATCONT [5].

conversion efficiency, ϵ, and microzooplankton natural mortality rate, μ, shifts the position of the saddle-node bifurcations to lower values of ξ, meaning that an increase in any one of these parameters will increase the possibility of phytoplankton bloom formation. Conversely, an increase in the microzooplankton grazing rate, g, phytoplankton half-saturation constant, k_0, copepod half-saturation constant, k_2, microzooplankton conversion efficiency, γ, or copepod mortality rate, δ, shifts the position of the saddle-node bifurcations to higher values of ξ, meaning that bloom formation is more difficult with an increase of these parameters.

Decreasing the microzooplankton grazing rate, g, from its fixed value causes a homoclinic orbit from the Hopf bifurcation to collide with the saddle-node curve, resulting in a Bogdanov-Takens bifurcation [22] at $g = 2.20\text{d}^{-1}$, $\xi = 0.075$ (BT in Figure 7b), following which the one-parameter bifurcation diagram for ξ has two limit points (saddle-node bifurcations) that are separated by a neutral saddle (Figure 8a). Decreasing the copepod mortality rate, δ, from its fixed value causes the Hopf and lower saddle-node bifurcation curves to intersect, resulting in a zero-Hopf bifurcation [22] at $\delta = 0.022$ d^{-1}, $\xi = 0.106$ (ZH in Figure 7j), following which the one-parameter bifurcation diagram for ξ has two limit points (saddle-node bifurcations) that are separated by a Hopf bifurcation (Figure 8b).

5. DISCUSSION

Here we have investigated the top-down role of infochemical-mediated predation in an NPMZ model that also includes the bottom-up effects of nutrient limitation.

In order to grow and reproduce, phytoplankton need light for energy as well as a wide range of dissolved macro- (e.g. nitrogen, phosphorus, silicon, sulfur, potassium and sodium) and micro-nutrients (e.g. iron, zinc, copper, manganese and vitamins) [19]. In the euphotic zone, the availability of a particular nutrient such as nitrogen, phosphorus or a trace metal, often becomes the limiting factor for phytoplankton growth [41]. Since phytoplankton need these nutrients in the appropriate ratios for synthesis of new molecules, one nutrient usually becomes depleted before the others and inhibits growth [41]. Here this important phenomenon was taken into account through construction of an NPMZ model that is closed to nutrients. For simplicity, Lewis et al. [24] constrained phytoplankton growth through use of the logistic growth function, which assumes a constant carrying capacity where phytoplankton are limited by their own biomass rather than by the availability of resources. Closing the system to nutrients is a more realistic way to model phytoplankton growth, where uptake removes nutrients from the dissolved nutrient pool, making them unavailable until death and remineralization from higher trophic levels.

For the sake of simplicity, the model constructed in this paper assumes total conservation of nutrients and can be considered analogous to interactions in a mesocosm. The model could be extended to consider an open sea scenario by incorporating diffusive mixing with a layer of deep water [e.g. 7, 8, 6]. However, our assumptions about copepod foraging relate to interactions at the meso-scale, where it is assumed that copepods are already in a patch of high biological activity and react to increases of infochemicals with an increase in foraging related behaviors. A water-column scale model of these interactions has been considered in [26].

For simplicity, Lewis et al. [24] considered a model of phytoplankton and microzooplankton dynamics where the effect of copepod predation was accounted for by the microzooplankton mortality terms, thereby limiting the validity of the model results to a few days. However, our assumption that any particulate nutrient stored in the plankton are immediately available as dissolved nutrients indicates longer time-scales as, in reality, the nutrient released following the death of the plankton will go to higher trophic levels or take time to decay or remineralize [2]. Hence, in this paper copepods were modeled explicitly to remove this contradiction between long and short time-scales. While the models are not directly comparable, our model does produce results that are qualitatively similar to those in [24]. The absence of infochemical-mediated predation ($\xi = 0$) resulted in unstable population dynamics. Increasing this parameter stabilizes the system and creates a region of bistability, where the ability of phytoplankton to bloom depends on the initial abundances of the modelled species. Further increasing ξ to 0.556 (when $T = 120\mu$g C l^{-1}) results in a single persistence equilibrium corresponding to high phytoplankton concentrations. In this situation, increased copepod predation on microzooplankton creates a grazing refuge for phytoplankton, allowing the formation of a bloom.

The only qualitative difference between our results and those in [24] is the position of the Hopf bifurcation. In [24] the Hopf bifurcation takes place before the first saddle-node bifurcation, meaning that the system is stabilised before exhibiting bistability. In our model the Hopf bifurcation occurs between the two saddle-node bifurcations (Figure 5), meaning that the system exhibits bistability before the equilibrium corresponding

to low phytoplankton biomass (E_{3L} in Figure 5) is stabilised. Lewis [23] analysed a model that is directly comparable to the model of Lewis et al. [24] using the same parameter values and found a similar discrepancy, which was due to the value of the half-saturation constant for phytoplankton uptake of nutrients. Lewis et al. [23] estimated the Michaelis-Menten parameters for phytoplankton growth from the values used for logistic growth in [24]. The maximum uptake rate of nutrients, v, for Michaelis-Menten growth and total amount of nutrients in the system, T, for nutrient conservation are analogous to the intrinsic phytoplankton growth rate, r, and carrying capacity, K, for logistic growth. However, logistic growth assumes a constant amount of nutrients available for uptake (dissolved N) rather than imposing a constraint on the total amount of nutrients in the system (particulate N + dissolved N). This means that the half saturation constant for phytoplankton uptake of nutrients, which determines the response of phytoplankton to nutrient availability [29], cannot be compared to a value in the logistic growth equation, where (dissolved) nutrient availability is assumed constant. It was shown that increasing the value of the half saturation constant in the NPM model of Lewis et al. [23] produced an analogous bifurcation diagram to that using logistic growth. Therefore it is likely that using a higher value of the half saturation constant for the phytoplankton uptake of nutrients (v) in our model would have a similar effect.

Food webs are controlled by both top-down and bottom-up processes. There has been a long-standing bias focusing on modelling bottom-up processes, such as nutrient limitation, when considering plankton ecosystems [39]. In such bottom-up trophic transfer models, for which the standard NPZ model is an example, nutrient supply governs primary production and herbivores are limited by the life cycles of the primary producer [33]. This is consistent with the Green World hypothesis, which proposes that the land is green because herbivore populations are limited by their predators and not their food [14]. However, Smetacek [33] argues that the fact oceans are blue, not green, implies phytoplankton are under mortality control exerted by grazers. This is reflected by the many defense mechanisms employed by phytoplankton [32]. This paper considers both bottom-up (nutrient limitation) and top-down control (infochemical-mediated predation). A key result of this work is that phytoplankton were able to bloom when a low infochemical-mediated predation value was compensated by a high total nutrient value, but were unable to bloom regardless of the level of infochemical-mediated predation when the total nutrient was too low, showing that the behavior of a top-down model is subject to change when bottom-up effects are directly included. A similar result was obtained by Vos et al. [40], who found the dynamical behaviour of a tritrophic model to change when prey employed inducible defences as the carrying capacity was varied. These results indicate that both bottom-up and top-down control play an important role in food-web dynamics, and are likely to extend beyond planktonic systems.

ACKNOWLEDGMENTS

This work was funded by a grant from the UK Natural Environment Research Council (NERC; NE/H009485/1).

REFERENCES

[1] S. D. Archer, C. E. Stelfox-Widdicombe, P. H. Burkill, and G. Malin. A dilution approach to quantify the production of dissolved dimethylsulphoniopropionate and dimethyl sulphide due to microzooplankton herbivory. *Aquat. Microb. Ecol.*, 23:131–145, 2001.

[2] N. F. Britton. *Essential Mathematical Biology*. Springer, London, 2003.

[3] S. Busenberg, S. K. Kumar, P. Austin, and G. Wake. The dynamics of a model of a plankton-nutrient interaction. *Bull. Math. Biol.*, 52:677–696, 1990.

[4] R. J. Charlson, J. E. Lovelock, M. O. Andreae, and S. G. Warren. Oceanic phytoplankton, atmospheric sulphur, cloud albedo and climate. *Nature*, 326:655–661, 1987.

[5] A. Dhooge, W. Govaerts, and Y. A. Kuznetsov. MATCONT: A MATLAB package for numerical bifurcation analysis of ODEs. *ACM T. Math. Software.*, 29:141–164, 2003.

[6] A. M. Edwards. Adding detritus to a nutrient-phytoplankton-zooplankton model: a dynamical-systems approach. *J. Plankton. Res*, 23:389–413, 2001.

[7] A. M. Edwards and J. Brindley. Oscillatory behaviour in a three-component plankton population model. *Dynam. Stabil. Syst.*, 11:347–370, 1996.

[8] A. M. Edwards and J. Brindley. Zooplankton mortality and the dynamical behaviour of plankton population models. *Bull. Math. Biol.*, 61:303–339, 1999.

[9] C. A. Edwards, H. P. Batchelder, and T. M. Powell. Modeling microzooplankton and macrozooplankton dynamics within a coastal upwelling system. *J. Plankton Res.*, 22:1619–1648, 2000.
[10] C. A. Edwards, T. A. Powell, and H. P. Batchelder. The stability of an NPZ model subject to realistic levels of vertical mixing. *J. Mar. Res.*, 58:37–60, 2000.
[11] C. S. Endres and K. J. Lohmann. Perception of dimethyl sulfide (DMS) by loggerhead sea turtles: a mechanism for locating high-productivity oceanic regions for foraging. *J. Exp. Biol.*, 215:3535–3538, 2012.
[12] P. J. S. Franks. Phytoplankton blooms in a fluctuating environment: the roles of plankton response time scales and grazing. *J. Plankton Res.*, 23:1433–1441, 2001.
[13] P. J. S. Franks. NPZ models of plankton dynamics: Their construction, coupling to physics, and application. *J. Oceanogr.*, 58:379–387, 2002.
[14] N. G. Hairston, F. E. Smith, and L. B. Slobodkin. Community structure, population control, and competition. *Am. Nat.*, 92:421–425, 1960.
[15] C. Hamm and V. Smetacek. Armor: why, when, and how? In P. G. Falkowski and A. H. Knoll, editors, *Evolution of Primary Producers in the Sea*, pages 311–332. Academic Press, Amsterdam, 2007.
[16] L. A. Hansson. Synergistic effects of food chain dynamics and induced behavioural responses in aquatic ecosystems. *Ecology*, 81:842–851, 2000.
[17] E. L. Harvey and S. Menden-Deuer. Predator-induced fleeing behaviors in phytoplankton: a new mechanism for harmful algal bloom formation? *PLoS ONE*, 7, 2012.
[18] C. S. Holling. The components of predation as revealed by a study of small mammal predation on the european pine sawfly. *Can. Entomol.*, 91:293–320, 1959.
[19] M. J. Kaiser, M. J. Attrill, S. Jennings, D. N. Thomas, D. K. A. Barnes, A. S. Brierley, J. G. Hiddink, H. Kaartokallio, N. V. C. Polunin, and D. G. Raffaelli. *Marine Ecology: Processes, Systems, and Impacts*. Oxford University Press, USA, second edition, 2011.
[20] T. Kiørboe. *A Mechanistic Approach to Plankton Ecology*. Princeton University Press, NJ, 2008.
[21] S. Kowalewsky, M. Dambach, B. Mauck, and G. Dehnhardt. High olfactory sensitivity for dimethyl sulphide in harbour seals. *Biol. Lett.*, 2:106–109, 2006.
[22] Y. A. Kuznetsov. *Elements of Applied Bifurcation Theory*. Springer, New York, second edition, 1998.
[23] N. D. Lewis. *Modelling the infochemical role of dimethylsulphide in pelagic multitrophic interactions*. PhD thesis, University of Essex, 2014.
[24] N. D. Lewis, M. N. Breckels, D. Archer, Steve, A. Morozov, J. W. Pitchford, M. Steinke, and E. A. Codling. Grazing-induced production of DMS can stabilize food-web dynamics and promote the formation of phytoplankton blooms in a multitrophic plankton model. *Biogeochemistry*, 110:303–313, 2012.
[25] N. D. Lewis, N. Breckels, Mark, M. Steinke, and E. A. Codling. Role of infochemical mediated zooplankton grazing in a phytoplankton competition model. *Ecol. Complex.*, 16:41–50, 2013.
[26] N. D. Lewis, A. Morozov, M. N. Breckels, M. Steinke, and E. A. Codling. Multitrophic interactions in the sea: assessing the effect of infochemical-mediated foraging in a 1-d spatial model. *Math. Model. Nat. Phenom.*, 8:25–44, 2013.
[27] G. Malin and G. O. Kirst. Algal production of dimethyl sulfide and its atmospheric role. *J. Phycol.*, 33:889–896, 1997.
[28] Maple 12. Maplesoft. A Division of Waterloo Maple Inc., 2008.
[29] C. B. Miller. *Biological Oceanography*. Blackwell Publishing, Oxford, 2004.
[30] A. Morozov, E. Arashkevich, A. Nikishina, and K. Solovyev. Nutrient-rich plankton community stabilized via predator-prey interactions: revisiting the role of vertical heterogeniety. *Math. Med. Biol.*, 28:185–215, 2011.
[31] G. A. Nevitt, R. R. Veit, and P. Kareiva. Dimethyl sulphide as a foraging cue for Antarctic Procellariiform seabirds. *Nature*, 376:680–682, 1995.
[32] V. Smetacek. A watery arms race. *Nature*, 411:745, 2001.
[33] V. Smetacek. Making sense of ocean biota: how evolution and biodiversity of land organisms differ from that of the plankton. *J. Biosci.*, 37:589–607, 2012.
[34] K. Soetaert, T. Petzoldt, and R. W. Setzer. Solving differential equations in R: Package deSolve. *J. Stat. Softw.*, 33:1–25, 2010.
[35] M. Steinke, G. Malin, and P. S. Liss. Trophic interactions in the sea: An ecological role for climate

relevant volatiles. *J. Phycol.*, 38:630–638, 2002.
[36] M. Steinke, J. Stefels, and E. Stamhuis. Dimethyl sulfide triggers search behaviour in copepods. *Limnol. Oceanogr.*, 51:1925–1930, 2006.
[37] S. L. Strom and T. A. Morello. Comparative growth rates and yields of ciliates and heterotrophic dinoflagellates. *J. Plankton. Res*, 20:571–584, 1998.
[38] J. T. Turner and P. A. Tester. Toxic marine phytoplankton, zooplankton grazers, and pelagic food webs. *Limnol. Oceanogr.*, 42:1203–1214, 1997.
[39] P. G. Verity and V. Smetacek. Organism life cycles, predation, and the structure of marine pelagic ecosystems. *Mar. Ecol. Prog. Ser.*, 130:277–293, 1996.
[40] M. Vos, B. W. Kooi, D. L. DeAngelis, and W. M. Mooji. Inducible defences and the paradox of enrichment. *OIKOS*, 105:471–480, 2004.
[41] R. G. Williams and M. J. Follows. *Ocean Dynamics and the Carbon Cycle*. Cambridge University Press, USA, 2011.
[42] G. V. Wolfe. The chemical defence ecology of marine unicellular plankton: constraints, mechanisms and impacts. *Biol. Bull.*, 198:225–244, 2000.
[43] G. V. Wolfe and M. Steinke. Grazing-activated production of dimethyl sulfide (DMS) by two clones of *Emiliania huxleyi*. *Limnol. Oceanogr.*, 41:1151–1160, 1996.